Physics Letters B 735 (2014) 288–294

Contents lists available at ScienceDirect

Physics Letters B

www.elsevier.com/locate/physletb

First πK atom lifetime and πK scattering length measurements

DIRAC Collaboration

B. Adeva [a], L. Afanasyev [b], Y. Allkofer [c], C. Amsler [d], A. Anania [e], S. Aogaki [f], A. Benelli [b], V. Brekhovskikh [g], T. Cechak [h], M. Chiba [i], P. Chliapnikov [g], C. Ciocarlan [f], S. Constantinescu [f], P. Doskarova [h], D. Drijard [j], A. Dudarev [b], M. Duma [f], D. Dumitriu [f], D. Fluerasu [f], A. Gorin [g], O. Gorchakov [b], K. Gritsay [b], C. Guaraldo [k], M. Gugiu [f], M. Hansroul [j], Z. Hons [l], S. Horikawa [c], Y. Iwashita [m], V. Karpukhin [b], J. Kluson [h], M. Kobayashi [n], V. Kruglov [b], L. Kruglova [b], A. Kulikov [b], E. Kulish [b], A. Kuptsov [b], A. Lamberto [e], A. Lanaro [o], R. Lednicky [p], C. Mariñas [a], J. Martincik [h], L. Nemenov [b,j], M. Nikitin [b], K. Okada [q], V. Olchevskii [b], M. Pentia [f], A. Penzo [r], M. Plo [a], T. Ponta [f], P. Prusa [h], G. Rappazzo [e], A. Romero Vidal [k], A. Ryazantsev [g], V. Rykalin [g], J. Saborido [a], J. Schacher [d,*], A. Sidorov [g], J. Smolik [h], S. Sugimoto [n], F. Takeutchi [q], L. Tauscher [s], T. Trojek [h], S. Trusov [t], T. Urban [h], T. Vrba [h], V. Yazkov [t], Y. Yoshimura [n], M. Zhabitsky [b], P. Zrelov [b]

[a] *Santiago de Compostela University, Spain*
[b] *JINR, Dubna, Russia*
[c] *Zurich University, Switzerland*
[d] *Albert Einstein Center for Fundamental Physics, Laboratory of High Energy Physics, Bern, Switzerland*
[e] *INFN, Sezione di Trieste and Messina University, Messina, Italy*
[f] *IFIN-HH, National Institute for Physics and Nuclear Engineering, Bucharest, Romania*
[g] *IHEP, Protvino, Russia*
[h] *Czech Technical University in Prague, Czech Republic*
[i] *Tokyo Metropolitan University, Japan*
[j] *CERN, Geneva, Switzerland*
[k] *INFN, Laboratori Nazionali di Frascati, Frascati, Italy*
[l] *Nuclear Physics Institute ASCR, Rez, Czech Republic*
[m] *Kyoto University, Kyoto, Japan*
[n] *KEK, Tsukuba, Japan*
[o] *University of Wisconsin, Madison, USA*
[p] *Institute of Physics ASCR, Prague, Czech Republic*
[q] *Kyoto Sangyo University, Kyoto, Japan*
[r] *INFN, Sezione di Trieste, Trieste, Italy*
[s] *Basel University, Switzerland*
[t] *Skobeltsin Institute for Nuclear Physics of Moscow State University, Moscow, Russia*

ARTICLE INFO

Article history:
Received 6 March 2014
Received in revised form 16 June 2014
Accepted 16 June 2014
Available online 20 June 2014
Editor: M. Doser

ABSTRACT

The results of a search for hydrogen-like atoms consisting of $\pi^{\mp}K^{\pm}$ mesons are presented. Evidence for πK atom production by 24 GeV/c protons from CERN PS interacting with a nickel target has been seen in terms of characteristic πK pairs from their breakup in the same target (178 ± 49) as well as in terms of produced πK atoms (653 ± 42). Using these results, the analysis yields a first value for the πK atom lifetime of $\tau = (2.5^{+3.0}_{-1.8})$ fs and a first measurement of the S-wave isospin-odd πK scattering length $|a_0^-| = \frac{1}{3}|a_{1/2} - a_{3/2}| = (0.11^{+0.09}_{-0.04})M_\pi^{-1}$ (a_I for isospin I).

* Corresponding author.

http://dx.doi.org/10.1016/j.physletb.2014.06.043

1. Introduction

In order to understand Quantum Chromodynamics (QCD) in the confinement region, low-energy QCD and specifically Chiral Perturbation Theory (ChPT) [1–4] has to be explored and tested experimentally. Pion–pion interaction at low energy is the simplest hadron–hadron process. The observation of dimesonic $\pi^+\pi^-$ atoms (pionium) has been reported in [5] and a measurement of their lifetime in [6].

A measurement of the πK atom[1] lifetime provides a direct determination of an S-wave πK scattering length difference [7]. This atom is an electromagnetically bound πK state with a Bohr radius of $a_B = 249$ fm and a ground state binding energy of $E_B = 2.9$ keV. It decays predominantly[2] by strong interaction into two neutral mesons $\pi^0 K^0$ or $\pi^0 \bar{K^0}$. The atom decay width $\Gamma_{\pi K}$ in the ground state (1S) is given by the relation [8]:

$$\Gamma_{\pi K} = \frac{1}{\tau} \simeq \Gamma\left(A_{K\pi} \to \pi^0 K^0 \text{ or } \pi^0 \bar{K^0}\right) = 8\alpha^3 \mu^2 p^* \left(a_0^-\right)^2 (1 + \delta_K). \quad (1)$$

The S-wave isospin-odd πK scattering length $a_0^- = \frac{1}{3}(a_{1/2} - a_{3/2})$, a_I for isospin I, is defined in pure QCD for quark masses $m_u = m_d$, α is the fine structure constant, $\mu = 109$ MeV/c^2 the reduced mass of the $\pi^\mp K^\pm$ system, $p^* = 11.8$ MeV/c the outgoing π^0 or K^0 ($\bar{K^0}$) momentum in the πK atom system, and δ_K accounts for corrections, due to isospin breaking, at order α and quark mass difference $(m_u - m_d)$.

There is a remarkable evolution from 1966 to 2004 in a_0^- calculation in ChPT and dispersion analysis in the presence of strange quarks [SU(3)]:

$$M_\pi a_0^- = 0.071\ (CA) \to 0.0793 \pm 0.0006\ (1l) \to 0.089\ (2l)^3 \to 0.090 \pm 0.005\ (dis). \quad (2)$$

CA denotes the current algebra value [1], $1l$ the prediction in SU(3) ChPT at the 1-*loop* level [9,10], $2l$ correspondingly at 2-*loop* [11] and *dis* the result of the dispersion analysis using Roy–Steiner equations [12] (M_π is charged pion mass). Furthermore, S-wave πK scattering has also been studied extensively in the framework of lattice QCD [13]. In a very recent paper [14] one can find the following promising results: $M_\pi a_{1/2} = 0.183 \pm 0.039$ and $M_\pi a_{3/2} = -0.0602 \pm 0.0040$ at physical pion and kaon masses, corresponding to $M_\pi a_0^- = 0.0811 \pm 0.0143$.

Inserting in (1) $M_\pi a_0^- = 0.090 \pm 0.005$ and $\delta_K = 0.040 \pm 0.022$ [8] one predicts for the πK atom lifetime

$$\tau = (3.5 \pm 0.4) \cdot 10^{-15}\ \text{s}. \quad (3)$$

This paper describes the first measurement of τ.

A method for producing and observing hadronic atoms has been developed [15] and successfully applied to $\pi^+\pi^-$ atoms [6]. The production yield of πK atoms in proton–nucleus collisions has been calculated for different proton energies and atom emission angles [16]. In the DIRAC experiment relativistic dimesonic bound states, formed by Coulomb final state interaction, propagate inside a target and can break up (Section 4). Particle pairs from breakup, called "atomic pairs" (atomic pair in Fig. 2), are characterised by small relative momenta, $Q < 3$ MeV/c, in the centre-of-mass (c.m.) system of the pair. Here, Q stands for the experimental c.m. relative momentum, smeared by multiple scattering in the target and other materials and by reconstruction uncertainties. Later, the original c.m. relative momentum q will also be used in the context of particle pair production.

The results of the first πK atom investigation have been published by DIRAC in 2009 [17]: $\pi^- K^+$ and $\pi^+ K^-$ pairs are produced in a 26 μm thick Pt target. An enhancement of πK pairs at low relative momentum is observed and corresponds to 173 ± 54 πK atomic pairs. The measured ratio of observed number of atomic pairs to number of produced atoms, the so-called breakup probability, allows to derive a lower limit on the πK atom lifetime of $\tau > 0.8 \cdot 10^{-15}$ s (90% CL). For a real lifetime measurement a target material like Ni should be used because of its breakup probability rapidly rising with lifetime around $3.5 \cdot 10^{-15}$ s.

Compared to the previous paper [17], we present the analysis of a larger data sample collected from a Ni target by the DIRAC setup. By including information from detectors upstream of the spectrometer magnet, the resolution in Q is improved.

2. Experimental setup

The apparatus [20] sketched in Fig. 1 detects and identifies $\pi^+\pi^-$, $\pi^- K^+$ and $\pi^+ K^-$ pairs with small Q. The structure of these pairs after the magnet is approximately symmetric for $\pi^+\pi^-$ and asymmetric for πK. Originating from a bound system these particles travel with the same velocity, and therefore for πK the kaon momentum is by a factor of about $\frac{M_K}{M_\pi} = 3.5$ larger than the pion momentum (M_K is charged kaon mass). The 2-arm magnetic spectrometer as presented is optimised for simultaneous detection of these pairs [18,19].

The 24 GeV/c primary proton beam from the CERN PS hits pure (99.98%) Ni targets with thicknesses of (98 ± 1) μm (Ni-1) in 2008 and (108 ± 1) μm (Ni-2) in 2009 and 2010. The radiation thickness of the 98 (108) μm Ni target amounts to $6.7 \cdot 10^{-3}$ ($7.4 \cdot 10^{-3}$) X_0 (radiation length), which is optimal for the lifetime measurement. The nuclear interaction probability for 98 (108) μm Ni is $6.4 \cdot 10^{-4}$ ($7.1 \cdot 10^{-4}$).

After the target station primary protons run forward to the beam dump, and the secondary channel with the whole setup is vertically inclined relative to the proton beam by 5.7° upward. Secondary particles are confined by the rectangular beam collimator inside of the second steel shielding wall, and the angular divergence in the horizontal (X) and vertical (Y) planes is ±1° and the solid angle $\Omega = 1.2 \cdot 10^{-3}$ sr. With a spill duration of 450 ms the beam intensity has been $(10.5–12) \cdot 10^{10}$ protons/spill and, correspondingly, the single counting rate in one plane of the ionisation hodoscope (IH) $(5–6) \cdot 10^6$ particles/spill. Secondary particles propagate mainly in vacuum up to the Al foil with a thickness of 0.68 mm ($7.6 \cdot 10^{-3} X_0$) at the exit of the vacuum chamber, which is located between the poles of the dipole magnet ($B_{max} = 1.65$ T and $BL = 2.2$ Tm).

In the vacuum gap MicroDrift Chambers (MDC) with 18 planes and a Scintillating Fiber Detector (SFD) with 3 planes (X, Y, U) have been installed to measure particle coordinates ($\sigma_{SFDx} = \sigma_{SFDy} = 60$ μm, $\sigma_{SFDu} = 120$ μm) and particle time ($\sigma_{tSFDx} = 380$ ps, $\sigma_{tSFDy} = \sigma_{tSFDu} = 520$ ps). The four IH planes serve to identify unresolved double tracks (signal only from one SFD column). The total matter radiation thickness between target and vacuum chamber amounts to $5.6 \cdot 10^{-2} X_0$.

Each spectrometer arm is equipped with the following subdetectors: drift chambers (DC) to measure particle coordinates with ≈85 μm precision; vertical hodoscope (VH) to measure time with 110 ps accuracy for particle identification via time-of-flight determination; horizontal hodoscope (HH) to select in the two

[1] The term πK atom or $A_{K\pi}$ refers to $\pi^- K^+$ and $\pi^+ K^-$ atoms.

[2] Further decay channels with photons and e^+e^- pairs are suppressed at $\mathcal{O}(10^{-3})$.

[3] No error is quoted in [11] because of unknown low-energy constants.

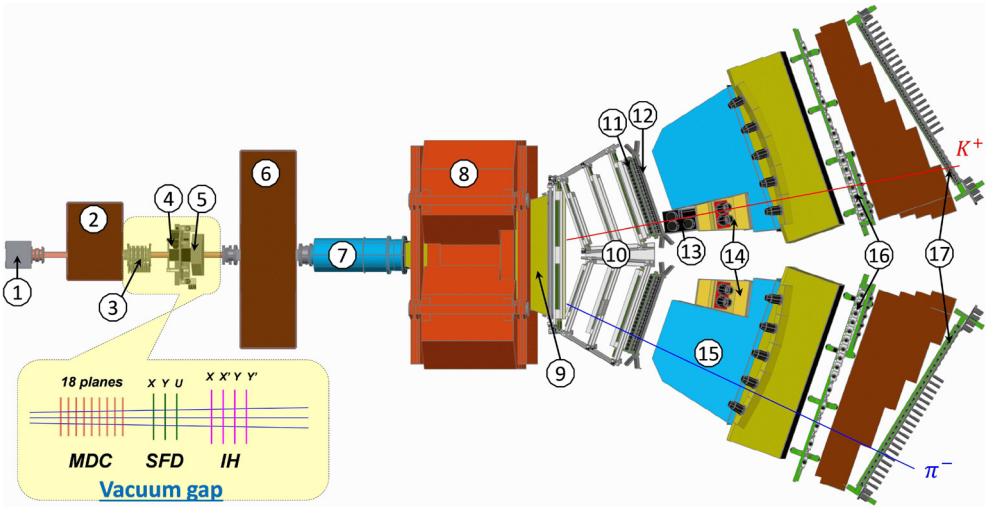

Fig. 1. General view of the DIRAC setup: 1 – target station; 2 – first shielding; 3 – microdrift chambers; 4 – scintillating fiber detector; 5 – ionisation hodoscope; 6 – second shielding; 7 – vacuum tube; 8 – spectrometer magnet; 9 – vacuum chamber; 10 – drift chambers; 11 – vertical hodoscope; 12 – horizontal hodoscope; 13 – aerogel Cherenkov; 14 – heavy gas Cherenkov; 15 – nitrogen Cherenkov; 16 – preshower; 17 – muon detector.

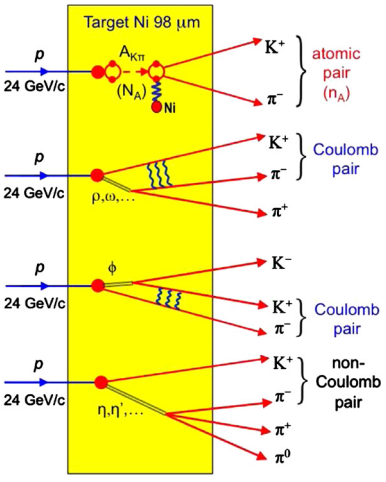

Fig. 2. Inclusive πK production in 24 GeV/c p–Ni interaction: $p + Ni \to \pi^{\mp} K^{\pm} + X$. The ionisation or breakup of πK atoms, $A_{K\pi}$, leads to so-called atomic pairs. (More details, see text.)

arms particles with vertical distances less than 75 mm (Q_Y less than 15 MeV/c); aerogel Cherenkov counter (ChA) to distinguish kaons from protons; heavy gas (C_4F_{10}) Cherenkov counter (ChF) to distinguish pions from kaons; nitrogen Cherenkov (ChN) and preshower (PSh) detector to identify e^+e^- pairs; iron absorber; two-layer muon scintillation counter (Mu) to identify muons. In the "negative" arm no aerogel counter has been installed, because the number of antiprotons is small compared to K^-.

Pairs of oppositely charged particles time-correlated (prompt pairs) and accidentals in the time interval ±20 ns are selected by requiring a 2-arm coincidence (ChN in anticoincidence) with a coplanarity restriction (HH) in the first-level trigger. The second-level trigger selects events with at least one track in each arm by exploiting DC-wire information (track finder). Using track information, the online trigger selects $\pi\pi$ and πK pairs with $|Q_X| < 12$ MeV/c and $|Q_L| < 30$ MeV/c.[4] The trigger efficiency is ≈98% for pairs with $|Q_X| < 6$ MeV/c, $|Q_Y| < 4$ MeV/c and $|Q_L| < 28$ MeV/c. For spectrometer calibration (geometry tuning and check of laboratory momentum resolution) π^-p ($\pi^+\bar{p}$) pairs from Λ ($\bar{\Lambda}$) decay have been used, and e^+e^- pairs to calibrate the relative time delays of VH, HH, SFD and IH and to measure the PSh rejection efficiency.

[4] The transverse ($Q_T = \sqrt{Q_X^2 + Q_Y^2}$) and longitudinal ($Q_L$) components of $\vec{Q}$ are defined with respect to the direction of the total laboratory pair momentum.

3. Production of bound and free $\pi^- K^+$ and $\pi^+ K^-$ pairs

Prompt $\pi^{\mp} K^{\pm}$ pairs from proton–nucleus collisions are produced directly or originate from short-lived (e.g. Δ, ρ), medium-lived (e.g. ω, ϕ) or long-lived (e.g. η', η) sources. Pion–kaon pairs produced directly, from short- or medium-lived sources undergo Coulomb final state interaction (Coulomb pair in Fig. 2) and so can form bound states. Pairs from long-lived sources are practically not affected by Coulomb interaction (non-Coulomb pair in Fig. 2). The accidental pairs are produced in different proton–nucleus interactions.

The cross section of πK atom production is given by the expression [15]:

$$\frac{d\sigma_A^n}{d\vec{p}_A} = (2\pi)^3 \frac{E_A}{M_A} \frac{d^2\sigma_s^0}{d\vec{p}_K d\vec{p}_\pi}\bigg|_{\frac{\vec{p}_K}{M_K} \approx \frac{\vec{p}_\pi}{M_\pi}} \cdot \left|\psi_n(0)\right|^2$$
$$= (2\pi)^3 \frac{E_A}{M_A} \frac{1}{\pi a_B^3 n^3} \frac{d^2\sigma_s^0}{d\vec{p}_K d\vec{p}_\pi}\bigg|_{\frac{\vec{p}_K}{M_K} \approx \frac{\vec{p}_\pi}{M_\pi}}, \quad (4)$$

where $\vec{p}_A$, E_A and M_A are the momentum, total energy and mass of the πK atom in the laboratory (lab) system, respectively, and $\vec{p}_K$ and $\vec{p}_\pi$ the momenta of the charged kaon and pion with equal velocities. Therefore, these momenta obey in good approximation the relations $\vec{p}_K = \frac{M_K}{M_A}\vec{p}_A$ and $\vec{p}_\pi = \frac{M_\pi}{M_A}\vec{p}_A$. The inclusive production cross section of πK pairs from short-lived sources without final state interaction (FSI) is denoted by σ_s^0, and $\psi_n(0)$ is the S-state atomic wave function at the origin with principal quantum number n. According to (4), πK atoms are only produced in S-states with probabilities $W_n = \frac{W_1}{n^3}$: $W_1 = 83.2\%$, $W_2 = 10.4\%$, $W_3 = 3.1\%$, …, $W_{n>3} = 3.3\%$.

In complete analogy, the free $\pi^{\mp} K^{\pm}$ pair production from short- and medium-lived sources (Coulomb pairs) is described – in the pointlike production approximation – in dependence of relative momentum q (Section 1) by

$$\frac{\mathrm{d}^2\sigma_C}{\mathrm{d}\vec{p}_K\mathrm{d}\vec{p}_\pi} = \frac{\mathrm{d}^2\sigma_s^0}{\mathrm{d}\vec{p}_K\mathrm{d}\vec{p}_\pi}\cdot A_C(q)$$
$$\text{with } A_C(q) = \frac{4\pi\mu\alpha/q}{1-\exp(-4\pi\mu\alpha/q)}. \quad (5)$$

The Coulomb enhancement function $A_C(q)$ is the well-known Sommerfeld–Gamow–Sakharov factor [21].

The relative yield of atoms to Coulomb pairs [22] is given by the ratio of (4) to (5). The total number N_A of produced πK atoms is determined by the model-independent relation

$$N_A = k(q_0)N_C(q \le q_0) \quad \text{with } k(q_0 = 3.12\ \text{MeV/c}) = 0.615, \quad (6)$$

where $N_C(q \le q_0)$ is the number of Coulomb pairs with relative momenta $q \le q_0$ and $k(q_0)$ a known function of q_0. By using the Monte Carlo (MC) technique, one can get the same relationship as in (6), but this time in terms of the experimental relative momentum Q.

So far, the pair production is assumed to be pointlike. In order to check for finite size effects due to the presence of medium-lived particles (ω, ϕ), a study of non-pointlike particle pair sources has been performed [23]. Due to the large value of the Bohr radius, $a_B = 249$ fm, the pointlike treatment of the Coulomb πK FSI is valid for directly produced pairs as well as for pairs from short-lived resonances. For π and K from medium-lived sources, corrections at the percent level have been applied to the production cross sections. Strong final state elastic and inelastic πK interactions are negligible.

4. Interaction of πK and $\pi\pi$ atoms with matter

While propagating through the target material, relativistic πK atoms can get excited or even ionised. The ionisation or breakup process competes with πK atom annihilation. The breakup probability P_{br} as a function of the atom lifetime τ, atom momentum p_A, target material and thickness has been extensively studied in the pionium case. In order to obtain $P_{\mathrm{br}}(\tau, p_A)$ for πK atoms at the 1% level, one has to take into account a series of projectile collisions with matter atoms along the path in the target, leading to transitions between various bound states or to breakup. For pionium, the resulting system of equations is solved exactly by eigendecomposition of the corresponding matrix [24,25] or by MC simulation [26]. The same approach can be applied for πK atoms.

In the present paper, we use a set of total and transition cross sections, calculated in the Born approximation for πK atoms interacting with Ni atoms, according to the method described in [24]. Solving the equation system, the breakup probability $P_{\mathrm{br}}(\tau)$ (Fig. 3) is obtained by convoluting $P_{\mathrm{br}}(\tau, p_A)$ with the experimental lab momentum spectra of small relative momentum πK Coulomb pairs. The function $P_{\mathrm{br}}(\tau)$ is used to extract a lifetime estimate from the measured πK atom breakup probability.

5. Data processing

Recorded events have been reconstructed with the DIRAC $\pi\pi$ analysis software modified for analysing πK data.

5.1. Tracking and setup tuning

Only events with one or two particle tracks in the DC of each arm are processed. Event reconstruction is performed according to the following steps: 1) One or two hadron tracks are identified in DC of each arm with hits in VH, HH and PSh slabs and no signal in ChN and Mu (Fig. 1). The earliest track in each arm is used for further analysis, because these tracks induce the trigger signal starting the readout procedure. 2) So-called DC tracks are extrapolated backward to the incident proton beam position on the target, using the transfer function of the DIRAC dipole magnet. This procedure provides approximated particle momenta and corresponding intersection points in MDC, SFD and IH. 3) Hits are searched around the expected SFD coordinates in the region defined by position accuracy (square region of side length ± 1 cm, corresponding to 3 to 5 σ). This way, events are selected with low and medium background defined by the following criteria: The number of hits around the two tracks is ≤ 4 in each SFD plane and ≤ 9 in all 3 SFD planes. These criteria reduce the data sample by 1/3. In order to find the best two-track combination, the momentum of the positive or negative particle may be modified to match the X-coordinates of tracks in DC and the SFD hits in the X- or U-plane. Furthermore, the two tracks may not use a common SFD hit in case of more than one hit in the proper region. In the final analysis, the combination with the best χ^2 in the other SFD planes is kept.

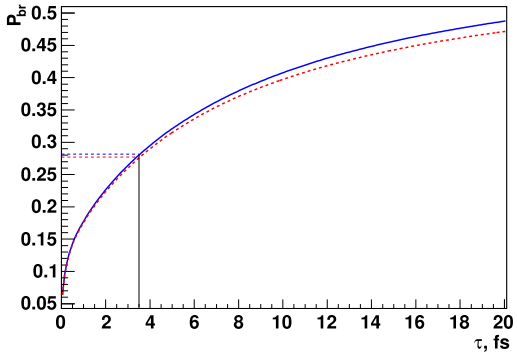

Fig. 3. Probability of πK atom breakup as a function of ground state lifetime τ in Ni targets of thicknesses 98 μm (Ni-1: dashed red) and 108 μm (Ni-2: solid blue). The predicted lifetime $\tau = 3.5 \cdot 10^{-15}$ s (Eq. (3)) corresponds to the breakup probability $P_{\mathrm{br}} = 0.28$.

To check and align the setup components, we take advantage of the $\Lambda \to \pi^-\mathrm{p}$ and $\bar{\Lambda} \to \pi^+\bar{\mathrm{p}}$ decays [27,28]. Using data from 2008 to 2010 and after geometrical alignment, the reconstructed Λ mass $[(1.115685 \pm 1.2 \cdot 10^{-6})\ \mathrm{GeV/c^2}]$ [29] agrees well with the PDG value $[(1.115683 \pm 6 \cdot 10^{-6})\ \mathrm{GeV/c^2}]$ [30]. The width of the Λ peak is a tool to evaluate the momentum resolution: it depends mainly on multiple scattering in the upstream setup part and the Al membrane at the exit of the vacuum chamber as well as on DC resolution and alignment. The upstream multiple scattering has been determined by analysing $\pi\pi$ events [31]. The MC simulation underestimates the Λ width by (6–7)% with respect to the experimental value, and this difference is consistent for each momentum bin and for Λ and $\bar{\Lambda}$. Hence, we attribute the discrepancy between experiment and simulation to an imperfect description of the downstream setup part. To fix it, a Gaussian smearing of the reconstructed momenta is introduced: $p^{smeared} = p(1 + C_f \cdot N(0,1))$. Smearing of simulated momenta with $C_f = (7 \pm 4) \cdot 10^{-4}$ leads to a Λ width in the reconstructed MC events, consistent with experimental data (Fig. 4). Using the decays $\Lambda \to \pi^-\mathrm{p}$ and $\bar{\Lambda} \to \pi^+\bar{\mathrm{p}}$ and taking into account momentum smearing, the momentum resolution has been evaluated as $\frac{dp}{p} = \frac{p_{gen}-p_{rec}}{p_{gen}}$ with p_{gen} and p_{rec} the generated and reconstructed momenta, respectively. Between 1.5 and 8 GeV/c, DIRAC is able to reconstruct particle momenta with a relative precision from $2.8 \cdot 10^{-3}$ to $4.4 \cdot 10^{-3}$. The following resolutions in (Q_X, Q_Y, Q_L) after the target are obtained by MC simulation: $\sigma_{Q_X} \approx \sigma_{Q_Y} \approx 0.18$ MeV/c, $\sigma_{Q_L} \approx 0.85$ MeV/c for $p_{\pi K} = p_\pi + p_K = 5$ GeV/c and about 6% higher values for $p_{\pi K} = 7.5$ GeV/c.

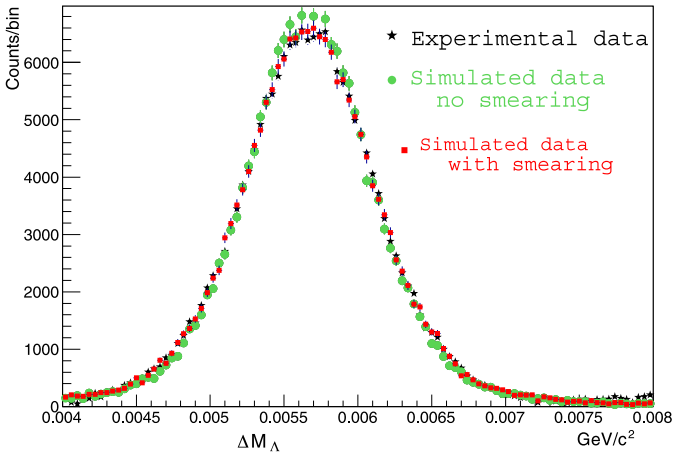

Fig. 4. Invariant π^-p mass distribution in the Λ region. [$\Delta M_\Lambda = M_\Lambda - 1.11$ GeV/c^2; green: MC distribution without smearing; red: MC with smearing of $7 \cdot 10^{-4}$; black: experimental data].

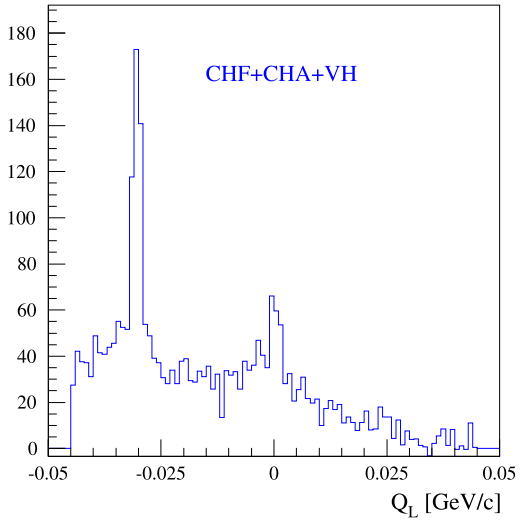

Fig. 5. Q_L distribution of potential π^-K^+ pairs after applying the selection described in the text. Events with positive Q_L are suppressed compared to those with negative Q_L due to lower acceptance and lower production cross section.

5.2. Event selection

Selected events are classified into three categories π^-K^+, π^+K^- and $\pi^+\pi^-$. The last category is used for calibration purposes. Pairs of πK are cleaned from $\pi^+\pi^-$, π^-p and $\pi^+\bar{p}$ background by the Cherenkov counters ChF and ChA. In the momentum range from 3.8 to 7 GeV/c, pions are detected by ChF with (95–97)% efficiency [32], whereas kaons and protons (antiprotons) do not produce a signal. The admixture of π^-p pairs is suppressed by the aerogel Cherenkov detector (ChA), which records kaons but not protons [33]. By requiring a signal in ChA and selecting compatible time-of-flights between target and VH, π^-p and $\pi^-\pi^+$ pairs, contaminating π^-K^+, can be substantially suppressed. Fig. 5 shows the well-defined π^-K^+ Coulomb peak at $Q_L = 0$ and the strongly suppressed peak from Λ decays at $Q_L = -30$ MeV/c. Similarly, Fig. 6 presents the π^+K^- Coulomb peak at $Q_L = 0$ and a second weaker peak from $\bar{\Lambda}$ decays at $Q_L = 30$ MeV/c.[5]

The final analysis sample contains only events which fulfil the following criteria:

[5] Note that $Q_L(\pi^+K^-) = -Q_L(\pi^-K^+)$ for the same p_K/p_π.

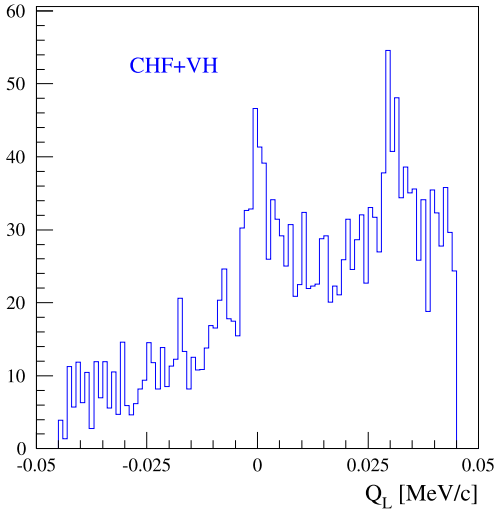

Fig. 6. Q_L distribution of potential π^+K^- pairs after selection. Events with negative Q_L are suppressed compared to those with positive Q_L due to acceptance and cross section.

$$|Q_X| < 6 \text{ MeV/c}, \qquad |Q_Y| < 4 \text{ MeV/c},$$
$$|Q_L| < 15 \text{ MeV/c}. \tag{7}$$

Due to finite detector efficiency, a certain admixture of misidentified pairs still remains in the experimental distribution. Their contribution (20 to 39%, depending on year and kaon sign) has been estimated by time-of-flight investigation and accordingly been subtracted [34].

6. Data simulation

The πK data samples consist of Coulomb, non-Coulomb and atomic pairs, and these event types have to be generated by MC in high statistics, i.e. the MC sample exceeds ten times the number of experimental events. The events are characterised by different q distributions: the non-Coulomb pairs are distributed in the low q region in accordance with phase space, while the q distribution of Coulomb pairs is modified by the factor $A_C(q)$. The q distribution of atomic pairs is given by the distribution of atomic states or quantum numbers at the breakup point in the target. The simulation procedure takes into account the measured lab pair momentum spectra, the detector response as well as multiple scattering in the target, the setup partitions and detector planes.

7. Data analysis

The analysis of πK data is similar to that of $\pi^+\pi^-$ data [6]: experimental distributions of relative momentum Q components have been fitted by simulated distributions of atomic, Coulomb and non-Coulomb pairs. Their corresponding numbers n_A, N_C and N_{nC} are free fit parameters. The relation between the numbers of produced atoms and Coulomb pairs (Section 3) allows to derive the breakup probability. The same procedure has been applied to π^-K^+ (Fig. 7) and π^+K^- (Fig. 8) pairs recorded from 2008 to 2010. The Q_L distributions shown are obtained from the 2-dimensional (Q_T, Q_L) distributions in the region $Q_T < 4$ MeV/c, $|Q_L| < 15$ MeV/c for pairs with lab momenta $4.8 < p_{\pi^-} + p_{K^+} < 7.2$ GeV/c and $4.8 < p_{\pi^+} + p_{K^-} < 7.6$ GeV/c. The different background conditions are taken into account. In the low Q_L region, one observes, as shown in Figs. 7 and 8, an excess of events (over free pairs), where atomic pairs are expected.

Similarly, the 1-dimensional (Q_L) distributions have been analysed with the results shown in Table 1. The 1- and 2-dimensional

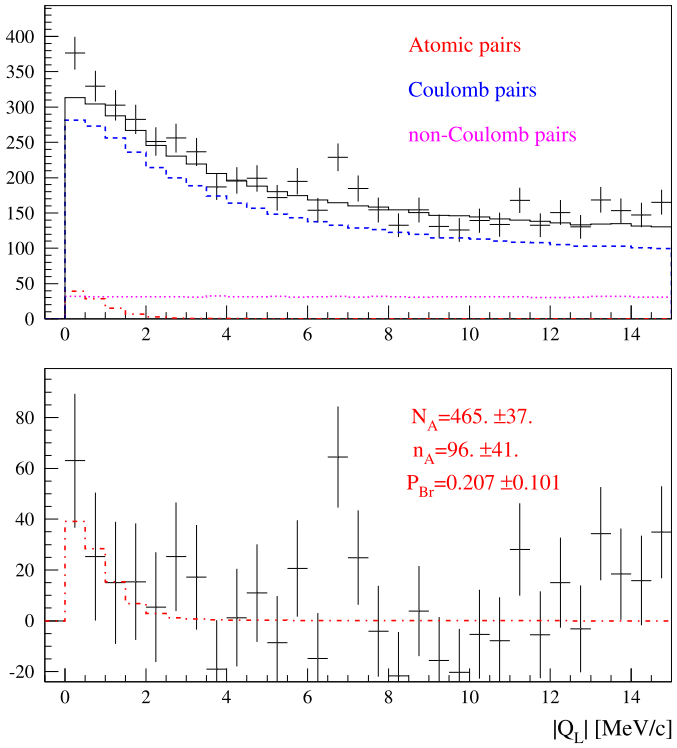

Fig. 7. Top: Experimental $|Q_L|$ distribution of $\pi^- K^+$ pairs fitted by the sum of simulated distributions of atomic, Coulomb and non-Coulomb pairs [2-dimensional (Q_T, Q_L) analysis with $\chi^2/n = 142/117$, n = number of degrees of freedom]. Atomic pairs are shown in red, and free pairs (Coulomb and non-Coulomb) in black. Bottom: Difference distribution between experimental and simulated free pair distributions compared with simulated atomic pairs. (For interpretation of the references to colour in this figure legend, the reader is referred to the web version of this article.)

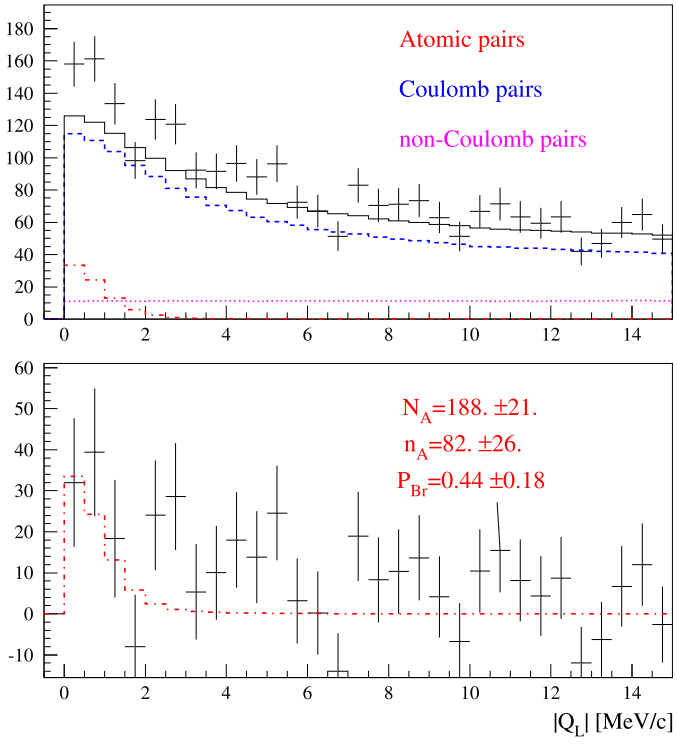

Fig. 8. Experimental $|Q_L|$ distributions for $\pi^+ K^-$ pairs analogous to Fig. 7 [fit quality $\chi^2/n = 130/117$].

Table 1
Results for N_A (number of produced atoms), n_A (number of atomic pairs) and $P_{\rm br}$ (breakup probability) by analysing 2-dimensional (Q_T, Q_L) and 1-dimensional (Q_L) distributions.

Year	N_A	n_A	$P_{\rm br}$
$\pi^- K^+$ over Q_T, Q_L			
2008	132 ± 16	14 ± 19	0.11 ± 0.15
2009	169 ± 24	33 ± 26	0.20 ± 0.17
2010	164 ± 23	49 ± 26	0.30 ± 0.19
$\pi^- K^+$ over Q_L			
2008	125 ± 19	25 ± 30	0.20 ± 0.26
2009	151 ± 28	54 ± 42	0.36 ± 0.33
2010	155 ± 28	61 ± 42	0.39 ± 0.32
$\pi^+ K^-$ over Q_T, Q_L			
2008	51 ± 11	21 ± 13	0.41 ± 0.33
2009	77 ± 13	26 ± 16	0.34 ± 0.24
2010	60 ± 12	35 ± 16	0.58 ± 0.36
$\pi^+ K^-$ over Q_L			
2008	47 ± 13	35 ± 21	0.75 ± 0.62
2009	76 ± 15	28 ± 24	0.37 ± 0.37
2010	83 ± 15	−4 ± 22	−0.04 ± 0.26

Table 2
Systematic errors in $P_{\rm br}$ common to all data collected from 2008 to 2010.

Sources of systematic errors	$\sigma^{\rm syst}_{Q_T,Q_L}$	$\sigma^{\rm syst}_{Q_L}$
Uncertainty in Λ width correction	$3.9 \cdot 10^{-3}$	$7.1 \cdot 10^{-3}$
Uncertainty of multiple scattering in Ni target	$3.2 \cdot 10^{-3}$	$5.4 \cdot 10^{-4}$
Accuracy of SFD simulation	$7.5 \cdot 10^{-4}$	$2.9 \cdot 10^{-4}$
Correction of Coulomb correlation function on finite size production region	$5.8 \cdot 10^{-5}$	$5.8 \cdot 10^{-5}$
Uncertainty in $P_{\rm br}(\tau)$ dependence	$5.0 \cdot 10^{-3}$	$5.0 \cdot 10^{-3}$
Uncertainty in target thickness	$3.0 \cdot 10^{-4}$	$< 3.0 \cdot 10^{-4}$

distributions have different sensitivities to sources of systematic errors [35]. Comparing the two outcomes allows to check the stability of our analysis procedure. The experimental conditions vary from 2008 to 2010, due to setup updates and beam quality. Table 1 summarises all the fit results of the data samples, analysed on the basis of 2- and 1-dimensional distributions. In total, the number of reconstructed atomic pairs from the 2-dimensional analysis amounts to $n_A(\pi^- K^+ + \pi^+ K^-) = 178 \pm 49$ (3.6 sigma). The extracted values for the breakup probability presented in Table 1 provide a means to estimate the πK atom lifetime.

8. Systematic errors

The evaluation of the breakup probability $P_{\rm br}$ is affected by several sources of systematic errors [34]. Most of them are induced by imperfections in the simulation of the different πK pairs, the atomic, Coulomb, non-Coulomb and misidentified pairs. Shape differences of experimental and simulated distributions in the fit procedure (Section 7) lead to biases on parameters, including breakup probability. The influence of error sources is different for the (Q_T, Q_L) and Q_L analyses. Table 2 shows systematic errors common to $\pi^- K^+$ and $\pi^+ K^-$, collected from 2008 to 2010. Other sources of systematic errors are uncertainties of the experimental lab momentum spectra of πK and background pairs. These spectra have been measured individually for the different run periods, producing systematic errors $\sigma^{\rm syst}_{\pi K}$ and $\sigma^{\rm syst}_{\rm back}$ in $P_{\rm br}$ (Table 3). The presented systematic errors have been included in estimating the πK atom lifetime as described in the next section.

9. Lifetime and scattering length measurements

The lifetime dependence of the breakup probability $P_{\rm br}(\tau, p_A)$ for $\pi^{\mp} K^{\pm}$ atoms with momentum p_A has been determined [25],

Table 3
Systematic errors in $P_{\rm br}$ specific to the data samples collected in 2008, 2009 and 2010.

Year	$\sigma^{\rm syst}_{\pi K}$	$\sigma^{\rm syst}_{\rm back}$
$K^+\pi^-$ over Q_T, Q_L		
2008	0.0028	0.0015
2009	0.0044	0.0025
2010	0.0036	0.0022
$K^+\pi^-$ over Q_L		
2008	0.0030	0.0028
2009	0.0053	0.0044
2010	0.0046	0.0036
π^+K^- over Q_T, Q_L		
2008	0.0072	0.0067
2009	0.0048	0.0028
2010	0.0017	0.0043
π^+K^- over Q_L		
2008	0.0093	0.0072
2009	0.0047	0.0048
2010	0.0021	0.0017

using total and excitation cross sections calculated in Born approximation [24]. Convoluting $P_{\rm br}(\tau, p_A)$ with the corresponding lab momentum spectra (Section 4 and [34]) leads to a set of $P_{{\rm br},i}(\tau)$ functions, each for every target thickness (Ni-1, Ni-2) and experimental spectrum (π^+K^-, π^-K^+). To estimate the ground state lifetime, the maximum likelihood method has been applied:

$$L(\tau) = \exp\left(-U^T G^{-1} U/2\right), \tag{8}$$

where U with $U_i = \Pi_i - P_{{\rm br},i}(\tau)$ is a vector of differences between measured Π_i ($P_{\rm br}$ in Table 1) and theoretical breakup probability $P_{{\rm br},i}(\tau)$ for data sample i. The matrix G, the error matrix of U, includes statistical and systematic uncertainties (Tables 2 and 3):

$$G_{ij} = \delta_{ij}\left[\left(\sigma^{\rm stat}_i\right)^2 + \left(\sigma^{\rm syst}_{\pi K,i}\right)^2 + \left(\sigma^{\rm syst}_{{\rm back},i}\right)^2\right] + \left(\sigma^{\rm syst}_{\rm global}\right)^2. \tag{9}$$

By combining the two charge combinations ($\pi^\mp K^\pm$) and considering the statistics collected from 2008 to 2010, the (Q_T, Q_L) analysis yields the following ground state lifetime estimation:

$$\tau = \left(2.5^{+3.0}_{-1.8}\big|_{\rm stat}{}^{+0.3}_{-0.1}\big|_{\rm syst}\right)\ {\rm fs} = \left(2.5^{+3.0}_{-1.8}\big|_{\rm tot}\right)\ {\rm fs}. \tag{10}$$

This experimental value agrees with the predicted one of Eq. (3).

The estimated ground state lifetime (10) corresponds to the πK scattering length (1)

$$\left|a_0^-\right| M_\pi = \frac{1}{3}|a_{1/2} - a_{3/2}| M_\pi = 0.107^{+0.093}_{-0.035} = 0.11^{+0.09}_{-0.04}, \tag{11}$$

to be compared with the theoretical predictions (2).

The Q_L analysis (Tables 1, 2 and 3) provides a similar estimation of the ground state lifetime, but with worse precision:

$$\tau = \left(2.4^{+5.4}_{-2.2}\big|_{\rm stat}{}^{+0.5}_{-0.1}\big|_{\rm syst}\right)\ {\rm fs} = \left(2.4^{+5.5}_{-2.2}\big|_{\rm tot}\right)\ {\rm fs}. \tag{12}$$

10. Conclusion

The analysis of πK pairs collected from 2008 to 2010 allows to evaluate the number of atomic πK pairs (178 ± 49) as well as the number of produced πK atoms (653 ± 42) and thus the breakup (ionisation) probability. By exploiting the dependence of breakup probability on atom lifetime, a value for the πK atom 1S lifetime $\tau = (2.5^{+3.0}_{-1.8})$ fs has been extracted. As the atom lifetime is related to a scattering length, a measurement of the S-wave isospin-odd πK scattering length $|a_0^-| = (0.11^{+0.09}_{-0.04})M_\pi^{-1}$ can be presented, which is compatible with theory.

Acknowledgements

We are grateful to R. Steerenberg and the CERN-PS crew for the delivery of a high quality proton beam and the permanent effort to improve the beam characteristics. The project DIRAC has been supported by the CERN and JINR administration, Ministry of Education and Youth of the Czech Republic by project LG130131, the Istituto Nazionale di Fisica Nucleare and the University of Messina (Italy), the Grant-in-Aid for Scientific Research from the Japan Society for the Promotion of Science, the Ministry of Education and Research (Romania), the Ministry of Education and Science of the Russian Federation and Russian Foundation for Basic Research, the Dirección Xeral de Investigación, Desenvolvemento e Innovación, Xunta de Galicia (Spain) and the Swiss National Science Foundation.

References

[1] S. Weinberg, Phys. Rev. Lett. 17 (1966) 616.
[2] J. Gasser, H. Leutwyler, Nucl. Phys. B 250 (1985) 465.
[3] B. Moussallam, Eur. Phys. J. C 14 (2000) 111.
[4] G. Colangelo, J. Gasser, H. Leutwyler, Nucl. Phys. B 603 (2001) 125.
[5] L. Afanasyev, et al., Phys. Lett. B 338 (1994) 478.
[6] B. Adeva, et al., Phys. Lett. B 704 (2011) 24.
[7] S.M. Bilen'kii, et al., Yad. Fiz. 10 (1969) 812;
S.M. Bilen'kii, et al., Sov. J. Nucl. Phys. 10 (1969) 469.
[8] J. Schweizer, Phys. Lett. B 587 (2004) 33.
[9] V. Bernard, N. Kaiser, U.-G. Meissner, Phys. Rev. D 43 (1991) 2757;
V. Bernard, N. Kaiser, U.-G. Meissner, Nucl. Phys. B 357 (1991) 129.
[10] B. Kubis, U.G. Meissner, Phys. Lett. B 529 (2002) 69.
[11] J. Bijnens, P. Dhonte, P. Talavera, J. High Energy Phys. 0405 (2004) 036.
[12] P. Buettiker, S. Descotes-Genon, B. Moussallam, Eur. Phys. J. C 33 (2004) 409.
[13] C.B. Lang, et al., Phys. Rev. D 86 (2012) 054508.
[14] K. Sasaki, et al., Phys. Rev. D 89 (2014) 054502.
[15] L. Nemenov, Yad. Fiz. 41 (1985) 980;
L. Nemenov, Sov. J. Nucl. Phys. 41 (1985) 629.
[16] O. Gorchakov, et al., Yad. Fiz. 63 (2000) 1936;
O. Gorchakov, et al., Phys. At. Nucl. 63 (2000) 1847.
[17] B. Adeva, et al., Phys. Lett. B 674 (2009) 11.
[18] O. Gorchakov, A. Kuptsov, DN(DIRAC-NOTE)-2005-05, cds.cern.ch/record/1369686.
[19] O. Gorchakov, DN-2005-23, cds.cern.ch/record/1369668.
[20] B. Adeva, et al., Updated CERN DIRAC spectrometer for dimeson atom investigation, Nucl. Instrum. Methods (2014), submitted for publication.
[21] A. Sakharov, Zh. Eksp. Teor. Fiz. 18 (1948) 631;
A. Sakharov, Sov. Phys. Usp. 34 (1991) 375.
[22] L. Afanasyev, O. Voskresenskaya, Phys. Lett. B 453 (1999) 302.
[23] R. Lednicky, J. Phys. G, Nucl. Part. Phys. 35 (2008) 125109.
[24] L. Afanasyev, A. Tarasov, Phys. At. Nucl. 59 (1996) 2130.
[25] M. Zhabitsky, Phys. At. Nucl. 71 (2008) 1040.
[26] C. Santamarina, et al., J. Phys. B 36 (2003) 4273.
[27] O. Gortchakov, DN-2009-10, cds.cern.ch/record/1369625;
O. Gortchakov, DN-2009-02, cds.cern.ch/record/1369633.
[28] B. Adeva, A. Romero, O. Vazquez Doce, DN-2005-16, cds.cern.ch/record/1369675.
[29] A. Benelli, V. Yazkov, DN-2013-03, cds.cern.ch/record/1622175.
[30] J. Beringer, et al., Particle Data Group, Phys. Rev. D 86 (2012) 010001.
[31] A. Benelli, V. Yazkov, DN-2012-04, cds.cern.ch/record/1475780.
[32] P. Doskarova, V. Yazkov, DN-2013-05, cds.cern.ch/record/1628541.
[33] A. Benelli, V. Yazkov, DN-2009-07, cds.cern.ch/record/1369628.
[34] V. Yazkov, M. Zhabitsky, DN-2013-06, cds.cern.ch/record/1628544.
[35] V. Yazkov, DN-2008-04, cds.cern.ch/record/1369641.